Front. Phys. 13(4), 138115 (2018)
https://doi.org/10.1007/s11467-018-0785-z

RESEARCH ARTICLE

Interfacial charge transfer in WS_2 monolayer/$CsPbBr_3$ microplate heterostructure

Zhen-Zhong Yan, Zhao-Han Jiang, Jun-Peng Lu†, Zhen-Hua Ni‡

School of Physics and Key Laboratory of MEMS of the Ministry of Education, Southeast University, Nanjing 211189, China
Corresponding authors. E-mail: †phyljp@seu.edu.cn, ‡zhni@seu.edu.cn
Received May 2, 2018; accepted May 12, 2018

Integration of heterogenous materials produces compelling physical phenomena and increased performance of optoelectronic devices. In this work, we integrate $CsPbBr_3$ microplate with WS_2 monolayer to investigate the interfacial carrier transfer mechanism in the heterojunction. The quenching of photoluminescence (PL) emission from $CsPbBr_3$ and WS_2 after heterostructure formation indicates efficient charge transfer in the junction. Low-temperature PL spectra reveal that the decreasing PL of WS_2 arises from the vanishing of biexcitons. Photodetection based on the WS_2/$CsPbBr_3$ heterostructure is demonstrated. The higher performance from the junction further certifies the occurrence of charge transfer in the heterojunction.

Keywords TMDs, inorganic perovskite, heterostructure, charge transfer

PACS numbers 78.67.-n, 71.35.-y, 73.40.Lq, 78.55.-m

1 Introduction

Two-dimensional (2D) transition metal dichalcogenides (TMDs) can be considered the semiconducting counterpart of graphene in the 2D limit. The growing interest in these 2D TMD systems is because these materials exhibit an intrinsic band gap and that the gap energy can be modified via physical or chemical processes [1–3]. Especially, the interesting indirect to direct band-gap transition renders monolayer TMDs as a significantly attractive material for a host of emerging optical and photoelectrical devices [4–11]. Integration of 2D TMDs with other materials such as rhodamine 6G [12], PbS quantum dots [13], single-walled carbon nanotubes [14], etc. to form heterostructures leads to the modification of the light–matter interactions in the material system. This would facilitate interesting phenomena in fundamental research as well as in practical applications.

Like TMDs, organolead halide perovskites are promising optoelectronic materials because of their large absorption coefficient, long free carrier diffusion length, and long lifetime. However, their instability restricts applications of organolead halide perovskites. The emergence of all-inorganic cesium lead halides with the formula $CsPbX_3$ (where X = halogen) overcomes this drawback [15]. In addition, $CsPbX_3$ exhibits a large variety of band structures with variation of stoichiometry, size, and dimension of materials [16]. Therefore, the integration of 2D TMDs with $CsPbX_3$ provides a platform to investigate the specific light–matter interactions and energy/charge transfer mechanisms in optoelectronics such as photodetectors. For this purpose, $CsPbX_3$ has been integrated with MoS_2 and graphene to improve light absorption and electron–hole pair separation, thereby the photoresponsivity of the photodetectors [17, 18]. In addition, the charge/energy transfer process in WS_2/$CsPbX_3$ heterostructures has been studied and the enhancement of photoluminescence (PL) emission from a WS_2 monolayer has been observed [19, 20].

Herein, to obtain deeper insight into the light–matter interactions in photodetectors based on TMDs/$CsPbX_3$ heterostructure, we integrate $CsPbBr_3$ microplates with a WS_2 monolayer to form a WS_2 monolayer/$CsPbBr_3$ microplate heterostructure. The compelling interfacial carrier dynamics is investigated by using PL spectra excited by lasers with different wavelengths. PL quenching is observed from both the $CsPbBr_3$ microplate and the WS_2 monolayer after formation of the heterostructure. Low-temperature PL spectra indicate that the charge transfer process rather than energy transfer occurs in

*Special Topic: Graphene and other Two-Dimensional Materials (Eds. Daria Andreeva, Wencai Ren, Guangcun Shan & Kostya Novoselov).

the heterostructure. The results agree well with the enhanced photodetection from the heterojunction.

2 Experimental methods

$CsPbBr_3$ microplates were synthesized via a chemical vapor deposition (CVD) process in a tube furnace. A piece of fresh-clave muscovite mica was used as a substrate. A powder of CsBr and $PbBr_2$ contained in a ceramic boat was mixed at a molar ratio of 1:1 and was inserted into the heating zone of the furnace. The tube chamber was pumped down to a base pressure of 2×10^{-3} mbar, and then high-purity Ar with a flow rate of 30 standard cubic centimeters per minute was introduced into the tube chamber. The system was ramped to 575 °C and maintained for 10 min. The pressure was stabilized at 80 mbar during the growth process. After that, the furnace was naturally cooled to room temperature. A WS_2 monolayer was mechanically exfoliated from the WS_2 crystal via an adhesive-tape-assisted approach. The WS_2 monolayer/$CsPbBr_3$ microplate heterostructure was prepared via a precise alignment and transfer process. First, $CsPbBr_3$ microplates were exfoliated from mica and transferred onto a piece of Si/SiO_2 substrate through the adhesive-tape-assisted approach. Then the WS_2 monolayer prepared onto polydimethylsiloxane was aligned and transferred onto the top of the $CsPbBr_3$ microplate under an optical microscope.

3 Results and discussion

Figure 1(a) illustrates an optical microscope (OM) image of the $CsPbBr_3$ microplates grown on mica substrate. Different colored microplates with well-defined square shapes are observed. The square shapes are determined by the intrinsic cubic structure of $CsPbBr_3$ formed at high temperature. van der Waals epitaxial growth makes exfoliation and transfer of the microplates via the adhesive-tape method possible. The different colors arising from different thicknesses of the microplates depend on the diffraction between the bottom and top surface of the plate. An atomic force microscopy (AFM) image of a typical microplate shows its thickness to be ∼ 180 nm [Fig. 1(b)]. $CsPbBr_3$ is a direct band-gap semiconductor. The as-grown microplate shows a strong absorption peak at ∼ 515.5 nm [Fig. 3(c)]. The band edge states of $CsPbBr_3$ are dominated by the hybridization states between the Br anion and the Pb cation orbitals of the inorganic $PbBr_6^+$ octahedron. The Tauc plot [insert of Fig. 3(c)] indicates that the band gap of the microplate is ∼ 2.35 eV. A strong and narrow PL emission peak is observed at ∼ 523 nm [2.37 eV, full width

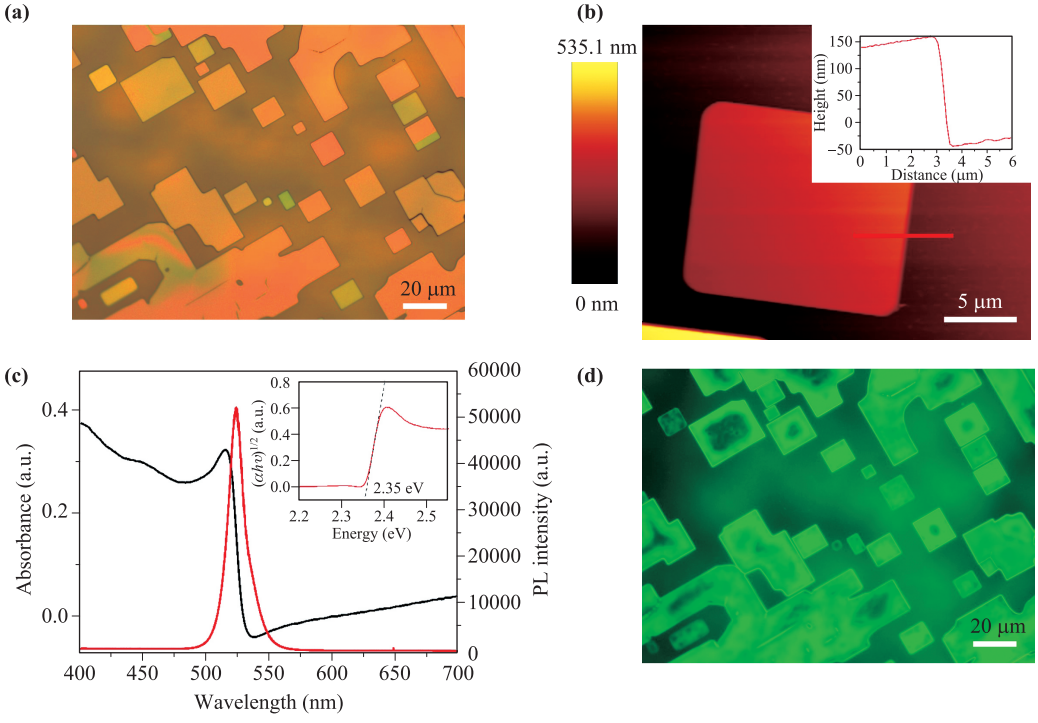

Fig. 1 **(a)** Optical image of the $CsPbBr_3$ microplates grown on mica. **(b)** AFM image of a typical $CsPbBr_3$ microplate. Inset shows the height profile of the microplate. **(c)** Absorption (black line) and PL (red line) spectra of the $CsPbBr_3$ microplates. Inset shows the Tauc plot of the absorbance spectrum. **(d)** Fluorescence image of the $CsPbBr_3$ microplates.

at half maximum (FWHM) ∼ 15.3 nm; Fig. 3(c)]. The Stokes shift is calculated to be ∼ 0.02 eV. The value of the FWHM is smaller than many of the II–VI group compound semiconductor nanostructures [21] and even smaller than those of $CsPbBr_3$ quantum dots or nanoparticles [22]. This indicates the high excitonic property of the as-grown microcrystals because the broadening of the PL linewidth is mainly from defects, surface disorders, and so forth [23–26]. The good optical property is also demonstrated by the fluorescent microscope (FM) image of the microplates [Fig. 1(d)]. Bright green emission is shown and the color information is consistent with the PL spectrum.

Figure 2(a) shows a piece of the WS_2 monolayer deposited on the Si/SiO_2 substrate. The height profile of ∼ 0.68 nm measured from the AFM image [Fig. 2(b)] indicates the monolayer feature of the sample. The four main phonon modes shown in the Raman spectrum in Fig. 2(c) indicate that the product is indeed a WS_2 monolayer because its chemical fingerprint is matched [27]. Another characteristic of a WS_2 monolayer is the strong PL emission [Fig. 2(d)]. With thickness reducing from the bulk to the monolayer, the band structure of the WS_2 will undergo a direct to indirect band-gap transition [28].

The WS_2 monolayer was then transferred and partially covered the $CsPbBr_3$ microplate, as shown by the OM image [Fig. 3(a)]. The overlapping region presents weaker fluorescent emission as compared to the bare $CsPbBr_3$ microplate [Fig. 3(b)]. For a more quantitative investigation, PL spectra are collected from the bare WS_2 monolayer, the bare $CsPbBr_3$ microplate, and the $WS_2/CsPbBr_3$ heterojunction, respectively. A 447-nm laser source was used as excitation light to generate the PL of the $CsPbBr_3$ microplate. Evidently, the peak position of $CsPbBr_3$ does not present an obvious shift, but the intensity shows a significant decrease after the heterojunction is formed under the same excitation conditions [Fig. 3(c)]. This is consistent with the observation from the FM image. Quenching of the PL of $CsPbBr_3$ after formation of heterojunction could arise from effective charge transfer or energy transfer [29]. In a previous report, energy transfer between the WS_2 monolayer and the $CsPbBr_3$ quantum dot heterostructure has been observed [19]. The occurrence of energy transfer would quench PL of the species with higher energy transition but enhance PL of the species with lower energy transition. Namely, it normally occurs in type-I heterojunctions. Therefore, a reduction of the PL signal from Cs_1PbBr_3 quantum dots and an increase of PL signal

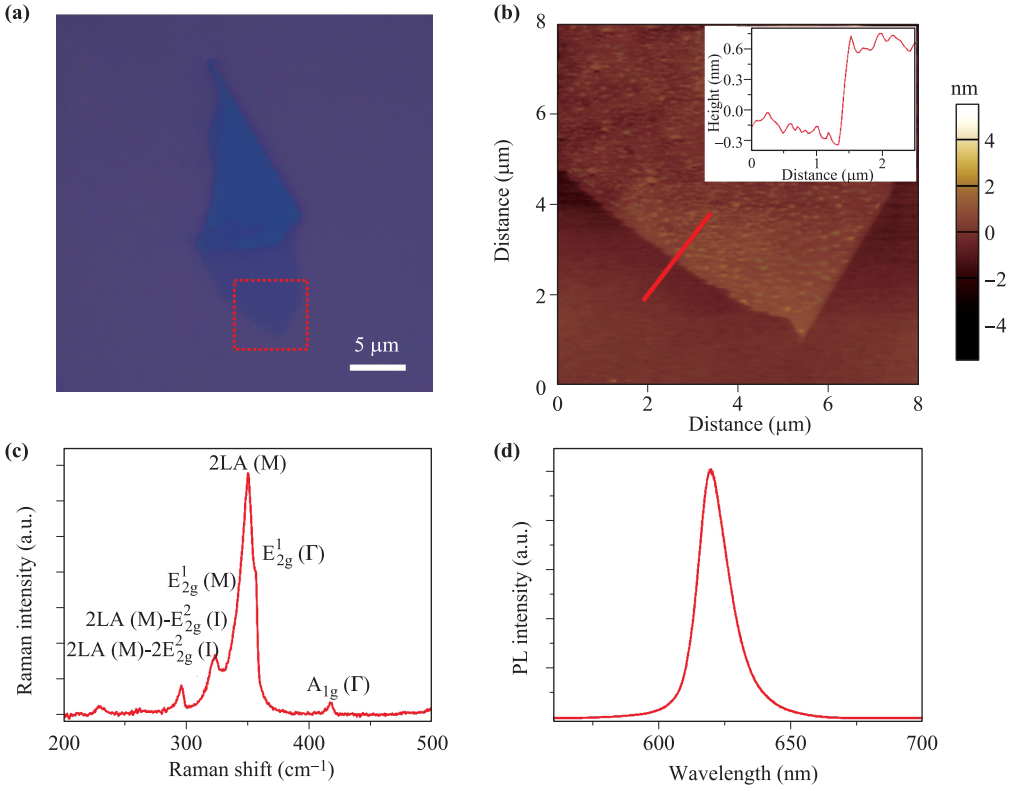

Fig. 2 **(a)** Optical image of a prepared WS_2 monolayer. **(b)** AFM image of the formed region in (a). **(c)** Raman and **(d)** PL spectra of the WS_2 monolayer.

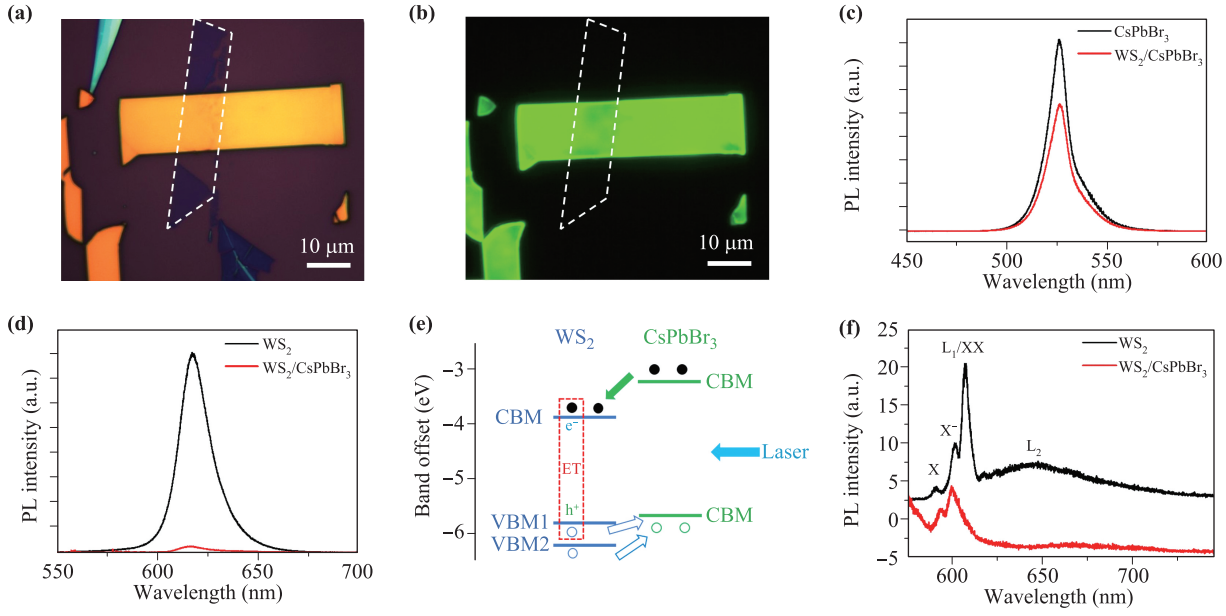

Fig. 3 **(a)** Optical and **(b)** fluorescence images of the $WS_2/CsPbBr_3$ heterostructure. **(c)** PL spectra of the bare $CsPbBr_3$ and $WS_2/CsPbBr_3$ heterostructure under 447 nm laser excitation at room temperature. **(d)** PL spectra of the bare WS_2 and $WS_2/CsPbBr_3$ heterostructure. **(e)** Schematic illustration of the band alignments in the heterostructure. **(f)** PL spectra of the bare WS_2 and $WS_2/CsPbBr_3$ heterostructure under 532 nm laser excitation at 3.3 K.

from WS_2 were found [19]. However, PL of the WS_2 monolayer is reduced instead of increased after formation of the heterojunction as revealed by our results, suggesting a different quenching mechanism.

To obtain clear insight into the dynamics behavior of the carriers between the WS_2 monolayer and $CsPbBr_3$ microplate, we further used a 532-nm laser to excite the sample and analyzed the spectra. In doing so, only the WS_2 monolayer became excited because the photon energy of the laser was not enough to generate excitons in $CsPbBr_3$. Therefore, the observed excitonic transition between these two materials is initiated from the WS_2 monolayer. Evidently, the PL intensity of the WS_2 monolayer is significantly reduced after formation of the heterojunction as compared to PL from bare WS_2 [Fig. 3(d)]. Because of the strong spin-orbit coupling, the valence band of the WS_2 monolayer presents a significant split. The valence band maximum (VBM) at the K point splits into two bands, denoted as VBM_1 and VBM_2, respectively. The conduction band minimum (CBM) and VBM of the WS_2 monolayer have been demonstrated to be -3.84 eV and -5.82 eV (VBM_1) and -6.25 eV (VBM_2), respectively [30]. According to the UPS measurements or density functional theory calculations, the CBM and VBM of $CsPbBr_3$ are located at ~ -3.30 to -3.35 eV and ~ -5.70 to -5.75 eV, respectively [17, 31]. Here, the quantum confinement effect is not considered as the thickness of our $CsPbBr_3$ microplate is > 100 nm. Therefore, the formed WS_2 monolayer/$CsPbBr_3$ microplate heterojunction is a typical type-II junction (whether VBM_1 or VBM_2) with a band offset of ~ 0.5 eV [Fig. 3(e)]. The excited excitons around the junction region prefer to be broken into free electrons and holes by the built-in potential. This results in a reduction of the PL intensity in both the $CsPbBr_3$ microplate and the WS_2 monolayer because the electrons are transferred to WS_2 and the holes are located inside $CsPbBr_3$. PL of the WS_2 monolayer was collected from the bare sample and the heterojunction at low temperature [3.3 K; Fig. 3(f)]. The three narrow peaks from left to right shown in the spectrum of bare WS_2 are ascribed to the recombination of neutral excitons, trions, and biexcitons. This is consistent with results from previous reports [32–34]. Under thermal equilibrium conditions, the density of biexcitons exhibits a quadratic relationship with the density of excitons [35]. This facilitates biexciton emission, making it the dominant peak in the spectrum. When charge transfer occurs in the heterojunction, the density of excitons significantly decreases. This indicates that the built-in potential of the heterojunction is sufficient to break the binding energy of biexcitons. Because the density of biexcitons varies quadratically with the density of excitons, under full thermal equilibrium conditions, the decrease of the biexciton emission will be more significant than the neutral exciton emission. Therefore, PL emission from the recombination of biexcitons vanishes with the occur-

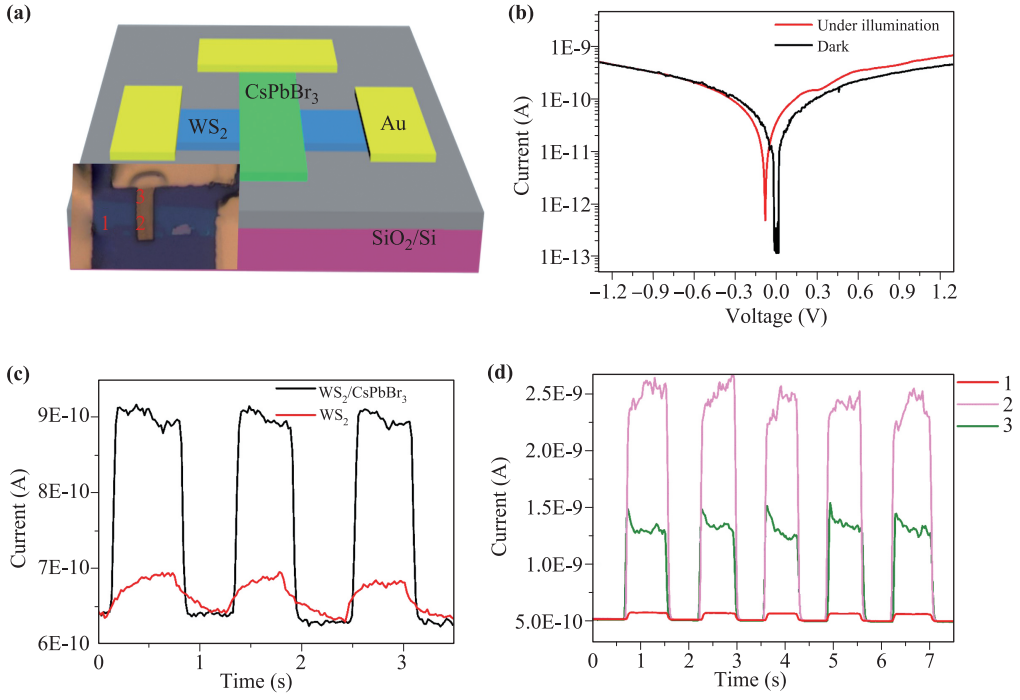

Fig. 4 **(a)** Schematic illustration of the $WS_2/CsPbBr_3$ photodetector. Inset shows the optical image of the device. **(b)** *I-V* characteristics of the output in dark and illumination conditions. **(c)** Photoswitching behavior of the bare WS_2 and heterostructure device at same conditions. **(d)** Photoreponse of the heterostructure device when light incident at different locations of the device as shown in the inset of (a).

rence of charge transfer.

The presence of charge transfer would facilitate WS_2 monolayer the efficient electron-collecting layer and $CsPbBr_3$ the hole-collecting layer in photodetection devices. In addition, the large absorption coefficient of perovskite would further improve light harvesting. A three-electrode device is demonstrated in Fig. 4(a). It includes the WS_2 channel and the $WS_2/CsPbBr_3$ channel. Figure 4(b) depicts the electrical outputs collected from the $WS_2/CsPbBr_3$ channel in the dark and under light illumination conditions. The slight shift of the characteristic curve under light illumination indicates the presence of a photovoltaic effect. This arises from the built-in potential of the heterojunction. The photoresponse on/off behaviors are collected from the $WS_2/CsPbBr_3$ channel and the WS_2 channel, respectively [Fig. 4(c)]. Evidently, a rapid on/off switching behavior is exhibited by the $WS_2/CsPbBr_3$ channel. It also presents a much higher photocurrent because of the direct contribution of charge transfer in the heterojunction. We then investigated the photoresponse from the $WS_2/CsPbBr_3$ channel when the laser was focused on different positions, as schematically illustrated in Fig. 4(a). Notably, the output of the device shows a maximum photocurrent when the laser irradiated the heterojunction. The fast response and the significant enhancement of the photocurrent from the heterojunction clearly demonstrate the efficient charge transfer process in the $WS_2/CsPbBr_3$ channel.

4 Conclusion

In summary, we have investigated the interfacial carrier transfer process between a $CsPbBr_3$ microplate and a WS_2 monolayer. A $WS_2/CsPbBr_3$ heterostructure was fabricated based on the mechanical exfoliated and CVD grown samples. Lasers with different wavelengths have been employed to excite PL from bare $CsPbBr_3$, WS_2, and the heterojunction, respectively. Quenching of the PL from both the $CsPbBr_3$ microplate and the WS_2 monolayer after formation of the heterostructure indicates the dominance of the charge transfer process. Photodetection from the heterojunction exhibits better performance than that from the bare WS_2 or $CsPbBr_3$. The enhancement arises from the efficient electron–hole pair separation. This is a direct demonstration of the occurrence of charge transfer.

Acknowledgements This work was supported by the National Natural Science Foundation of China (Grant Nos. 61774034,

11704068, and 61422503), the Open Research Fund of Key Laboratory of MEMS of Ministry of Education (SEU, China), and the Fundamental Research Funds for the Central Universities.

References

1. Editorial, Graphene is not alone, *Nat. Nanotechnol.* 7(11), 683 (2012)
2. Z. Hu, Z. Wu, C. Han, J. He, Z. Ni, and W. Chen, Two-dimensional transition metal dichalcogenides: Interface and defect engineering, *Chem. Soc. Rev.* 47(9), 3100 (2018)
3. Y. Lee, X. Zhang, W. Zhang, M. Chang, C. Lin, K. Chang, Y. Yu, J. T. Wang, C. Chang, L. Li, and T. Lin, Synthesis of large-area MoS_2 atomic layers with chemical vapor deposition, *Adv. Mater.* 24(17), 2320 (2012)
4. A. M. Jones, H. Yu, N. J. Ghimire, S. Wu, G. Aivazian, J. S. Ross, B. Zhao, J. Yan, D. G. Mandrus, D. Xiao, W. Yao, and X. Xu, Optical generation of excitonic valley coherence in monolayer WSe_2, *Nat. Nanotechnol.* 8(9), 634 (2013)
5. H. Zeng, J. Dai, W. Yao, D. Xiao, and X. Cui, Valley polarization in MoS_2 monolayers by optical pumping, *Nat. Nanotechnol.* 7(8), 490 (2012)
6. K. F. Mak, K. He, J. Shan, and T. F. Heinz, Control of valley polarization in monolayer MoS_2 by optical helicity, *Nat. Nanotechnol.* 7(8), 494 (2012)
7. T. Cao, G. Wang, W. Han, H. Ye, C. Zhu, J. Shi, Q. Niu, P. Tan, E. Wang, B. Liu, and J. Feng, Valley-selective circular dichroism of monolayer molybdenum disulphide, *Nat. Commun.* 3(1), 887 (2012)
8. J. S. Ross, P. Klement, A. M. Jones, N. J. Ghimire, J. Yan, D. G. Mandrus, T. Taniguchi, K. Watanabe, K. Kitamura, W. Yao, D. H. Cobden, and X. Xu, Electrically tunable excitonic light-emitting diodes based on monolayer WSe_2 p–n junctions, *Nat. Nanotechnol.* 9(4), 268 (2014)
9. A. Pospischil, M. M. Furchi, and T. Mueller, Solar-energy conversion and light emission in an atomic monolayer p–n diode, *Nat. Nanotechnol.* 9(4), 257 (2014)
10. W. Wang, R. Du, X. Guo, J. Jiang, W. Zhao, Z. Ni, X. Wang, Y. You, and Z. Ni, Interfacial amplification for graphene-based position-sensitive-detectors, *Light Sci. Appl.* 6(10), e17113 (2017)
11. J. Lu, J. H. Lu, H. Liu, B. Liu, K. X. Chan, J. Lin, W. Chen, K. P. Loh, and C. H. Sow, Improved photoelectrical properties of MoS_2 films after laser micromachining, *ACS Nano* 8(6), 6334 (2014)
12. S. H. Yu, Y. Lee, S. K. Jang, J. Kang, J. Jeon, C. Lee, J. Y. Lee, H. Kim, E. Hwang, S. Lee, and J. H. Cho, Dye-sensitized MoS_2 photodetector with enhanced spectral photoresponse, *ACS Nano* 8(8), 8285 (2014)
13. D. Kufer, I. Nikitskiy, T. Lasanta, G. Navickaite, F. H. L. Koppens, and G. Konstantatos, Hybrid 2D-0D MoS_2-PbS quantum dot photodetectors, *Adv. Mater.* 27(1), 176 (2015)
14. D. Jariwala, V. K. Sangwan, C. C. Wu, P. L. Prabhumirashi, M. L. Geier, T. J. Marks, L. J. Lauhon, and M. C. Hersam, Gate-tunable carbon nanotube-MoS_2 heterojunction p-n diode, *Proc. Natl. Acad. Sci. USA* 110(45), 18076 (2013)
15. S. Yakunin, L. Protesescu, F. Krieg, M. I. Bodnarchuk, G. Nedelcu, M. Humer, G. De Luca, M. Fiebig, W. Heiss, and M. V. Kovalenko, Low-threshold amplified spontaneous emission and lasing from colloidal nanocrystals of caesium lead halide perovskites, *Nat. Commun.* 6(1) (2015)
16. V. K. Ravi, G. B. Markad, and A. Nag, Band edge energies and excitonic transition probabilities of colloidal $CsPbX_3$ (X = Cl, Br, I) perovskite nanocrystals, *ACS Energy Lett.* 1(4), 665 (2016)
17. X. Song, X. Liu, D. Yu, C. Huo, J. Ji, X. Li, S. Zhang, Y. Zou, G. Zhu, Y. Wang, M. Wu, A. Xie, and H. Zeng, Boosting two-dimensional $MoS_2/CsPbBr_3$ photodetectors via enhanced light absorbance and interfacial carrier separation, *ACS Appl. Mater. Inter.* 10(3), 2801 (2018)
18. D. Kwak, D. Lim, H. Ra, P. Ramasamy, and J. Lee, High performance hybrid graphene–$CsPbBr_{3-x}I_x$ perovskite nanocrystal photodetector, *RSC Adv.* 6(69), 65252 (2016)
19. H. Li, X. Zheng, Y. Liu, Z. Zhang, and T. Jiang, Ultrafast interfacial energy transfer and interlayer excitons in the monolayer $WS_2/CsPbBr_3$ quantum dot heterostructure, *Nanoscale* 10(4), 1650 (2018)
20. Y. Liu, H. Li, X. Zheng, X. Cheng, and T. Jiang, Giant photoluminescence enhancement in monolayer WS_2 by energy transfer from $CsPbBr_3$ quantum dots, *Opt. Mater. Express* 7(4), 1327 (2017)
21. H. W. Liu, J. P. Lu, H. M. Fan, C. H. Sow, S. H. Tang, and X. H. Zhang, Temperature and composition dependence of photoluminescence dynamics in CdS_xSe_{1-x} ($0 \leq x \leq 1$) nanobelts, *J. Appl. Phys.* 111(7), 073112 (2012)
22. L. Protesescu, S. Yakunin, M. I. Bodnarchuk, F. Krieg, R. Caputo, C. H. Hendon, R. X. Yang, A. Walsh, and M. V. Kovalenko, Nanocrystals of cesium lead halide perovskites ($CsPbX_3$, X = Cl, Br, and I): Novel optoelectronic materials showing bright emission with wide color gamut, *Nano Lett.* 15(6), 3692 (2015)
23. V. D. Innocenzo, G. Grancini, M. J. P. Alcocer, A. R. S. Kandada, S. D. Stranks, M. M. Lee, G. Lanzani, H. J. Snaith, and A. Petrozza, Excitons versus free charges in organo-lead tri-halide perovskites, *Nat. Commun.* 5, 3586 (2014)
24. G. Moody, C. Kavir Dass, K. Hao, C. Chen, L. Li, A. Singh, K. Tran, G. Clark, X. Xu, G. Berghäuser, E. Malic, A. Knorr, and X. Li, Intrinsic homogeneous

linewidth and broadening mechanisms of excitons in monolayer transition metal dichalcogenides, *Nat. Commun.* 6(1), 8315 (2015)

25. G. Grosso, J. Graves, A. T. Hammack, A. A. High, L. V. Butov, M. Hanson, and A. C. Gossard, Excitonic switches operating at around 100 K, *Nat. Photonics* 3(10), 577 (2009)
26. T. Byrnes, N. Y. Kim, and Y. Yamamoto, Exciton–polariton condensates, *Nat. Phys.* 10(11), 803 (2014)
27. A. Berkdemir, H. R. Gutiérrez, A. R. Botello-Méndez, N. Perea-López, A. L. Elías, C. Chia, B. Wang, V. H. Crespi, F. López-Urías, J. Charlier, H. Terrones, and M. Terrones, Identification of individual and few layers of WS_2 using Raman spectroscopy, *Sci. Rep.* 3(1), 1755 (2013)
28. J. Lu, H. Liu, E. S. Tok, and C. Sow, Interactions between lasers and two-dimensional transition metal dichalcogenides, *Chem. Soc. Rev.* 45(9), 2494 (2016)
29. X. Hong, J. Kim, S. Shi, Y. Zhang, C. Jin, Y. Sun, S. Tongay, J. Wu, Y. Zhang, and F. Wang, Ultrafast charge transfer in atomically thin MoS_2/WS_2 heterostructures, *Nat. Nanotechnol.* 9(9), 682 (2014)
30. G. Liu, W. Shan, Y. Yao, W. Yao, and D. Xiao, Three-band tight-binding model for monolayers of group-VIB transition metal dichalcogenides, *Phys. Rev. B* 88(8), 085433 (2013)
31. M. Kulbak, S. Gupta, N. Kedem, I. Levine, T. Bendikov, G. Hodes, and D. Cahen, Cesium enhances long-term stability of lead bromide perovskite-based solar cells, *J. Phys. Chem. Lett.* 7(1), 167 (2016)
32. H. Liu, J. Lu, K. Ho, Z. Hu, Z. Dang, A. Carvalho, H. R. Tan, E. S. Tok, and C. H. Sow, Fluorescence concentric triangles: A case of chemical heterogeneity in WS_2 atomic monolayer, *Nano Lett.* 16(9), 5559 (2016)
33. M. S. Kim, S. J. Yun, Y. Lee, C. Seo, G. H. Han, K. K. Kim, Y. H. Lee, and J. Kim, Biexciton emission from edges and grain boundaries of triangular WS_2 monolayers, *ACS Nano* 10(2), 2399 (2016)
34. A. Venkatakrishnan, H. Chua, P. Tan, Z. Hu, H. Liu, Y. Liu, A. Carvalho, J. Lu, and C. H. Sow, Microsteganography on WS_2 monolayers tailored by direct laser painting, *ACS Nano* 11(1), 713 (2017)
35. J. C. Kim, D. R. Wake, and J. P. Wolfe, Thermo dynamics of biexcitons in a GaAs quantum well, *Phys. Rev. B* 50(20), 15099 (1994)